

Article

The E3 Ubiquitin Ligase ATL9 Affects Expression of Defense Related Genes, Cell Death and Callose Deposition in Response to Fungal Infection

Tingwei Guo ^{1,2,†}, Feng Kong ^{1,†} , Carter Burton ¹, Steven Scaglione ¹ , Blake Beagles ¹, Justin Ray ¹ and Katrina M. Ramonell ^{1,*}

¹ Department of Biological Sciences, The University of Alabama, Tuscaloosa, AL 35401, USA; tingweig@usc.edu (T.G.); fkong@crimson.ua.edu (F.K.); cdburton1@crimson.ua.edu (C.B.); steven.r.scaglione@vanderbilt.edu (S.S.); abbeagles@crimson.ua.edu (B.B.); jbray5@crimson.ua.edu (J.R.)

² Center for Craniofacial Molecular Biology, University of Southern California, Los Angeles, CA 90089, USA

* Correspondence: kramonell@ua.edu

† These authors contributed equally to this work.

Abstract: Plants use diverse strategies to defend themselves from biotic stresses in nature, which include the activation of defense gene expression and a variety of signal transduction pathways. Previous studies have shown that protein ubiquitination plays a critical role in plant defense responses, however the details of its function remain unclear. Our previous work has shown that increasing expression levels of *ATL9*, an E3 ubiquitin ligase in *Arabidopsis thaliana*, increased resistance to infection by the fungal pathogen, *Golovinomyces cichoracearum*. In this study, we demonstrate that the defense-related proteins PDF1.2, PCC1 and FBS1 directly interact with ATL9 and are targeted for degradation to the proteasome by ATL9. The expression levels of *PDF1.2*, *PCC1* and *FBS1* are decreased in T-DNA insertional mutants of *atl9* and T-DNA insertional mutants of *pdf1.2*, *pcc1* and *fbs1* are more susceptible to fungal infection. In addition, callose is more heavily deposited at infection sites in the mutants of *atl9*, *fbs1*, *pcc1* and *pdf1.2*. Overexpression of *ATL9* and of mutants in *fbs1*, *pcc1* and *pdf1.2* showed increased levels of cell death during infection. Together these results indicate that ubiquitination, cell death and callose deposition may work together to enhance defense responses to fungal pathogens.

Keywords: plant defense; ubiquitination; fungal infection; plant-pathogen interaction; signal transduction pathways; E3 ubiquitin ligase; *Arabidopsis thaliana*



Citation: Guo, T.; Kong, F.; Burton, C.; Scaglione, S.; Beagles, B.; Ray, J.; Ramonell, K.M. The E3 Ubiquitin Ligase ATL9 Affects Expression of Defense Related Genes, Cell Death and Callose Deposition in Response to Fungal Infection. *Pathogens* **2022**, *11*, 68. <https://doi.org/10.3390/pathogens11010068>

Academic Editor: Xiangming Xu

Received: 18 November 2021

Accepted: 31 December 2021

Published: 5 January 2022

Publisher's Note: MDPI stays neutral with regard to jurisdictional claims in published maps and institutional affiliations.



Copyright: © 2022 by the authors. Licensee MDPI, Basel, Switzerland. This article is an open access article distributed under the terms and conditions of the Creative Commons Attribution (CC BY) license (<https://creativecommons.org/licenses/by/4.0/>).

1. Introduction

Plants face a variety of fungal pathogens in nature, which pose significant threats to successful growth and reproduction [1]. Unlike animals, plants lack a sophisticated adaptive immune system. Instead, plants have evolved diverse strategies to recognize pathogens and defend against them [1]. Our current view of the plant immune system can be represented as a 'zigzag' model with two layers [2]. The first layer of the immune system involves the recognition of conserved molecules from pathogens (pathogen-associated or microbe-associated molecular patterns, PAMPs or MAMPs), by plant transmembrane pattern recognition receptors (PRRs) that induces pattern-triggered immunity (PTI) [3]. However, pathogens that successfully colonize host plants can deliver virulence factors (effectors) into plant cells to counteract the effects of plant PTI, referred to as effector-triggered susceptibility (ETS) [2]. In this case, the second layer of the plant immune system comes into play which involves the recognition of effectors by plant nucleotide-binding leucine-rich repeat (NB-LRR) proteins, resulting in effector-triggered immunity (ETI) [4]. Both PTI and ETI activate complex immune responses, including the generation of reactive oxygen species, induction of phosphorylation cascades, the hypersensitive response (HR),

the deposition of callose, and the production of antimicrobial compounds and defense hormones [5,6].

Such complex immune responses require tight regulation and coordination. The Ubiquitin/26S proteasome system plays an important role in degrading cellular proteins and maintaining protein homeostasis in both plants and animals. In recent years it has also emerged as one of the major regulatory signals in plant-fungal interactions [7]. The covalent linkage of ubiquitin, a 76-amino-acid-long protein, to a target protein is a key step in protein degradation via the ubiquitin proteasome system. In general, protein ubiquitination is mediated by three essential enzymes: ubiquitin-activating enzymes (E1), ubiquitin-conjugating enzymes (E2), and ubiquitin ligases (E3). E3 ligases are responsible for recognizing and ubiquitinating specific proteins, thus targeting them for degradation to the proteasome [8]. In *Arabidopsis* there are more than 1300 genes that are predicted to encode E3 ligases while E1 and E2 enzymes are encoded by only 2 and 37 genes, respectively [9]. The large number and diversity of E3 ligases allow for response specificity in different signaling pathways. Current research classifies plant E3 ligases into four main categories based on their structural features and mechanism of action: HECT (Homologous to E6-associated protein C-Terminus), RING (Really Interesting New Gene), U-Box, and CRL (Cullin-RING Ligases) [10]. Although many studies have shown that ubiquitin ligases play a critical role in plant defense, the detailed functions and regulation of these enzymes remains unclear.

In *Arabidopsis thaliana* the ATL9 protein is an E3 ubiquitin ligase that is induced by chitin and involved in basal resistance to the biotrophic fungal pathogen, *Golovinomyces cichoracearum*, the causal agent of powdery mildew disease [11,12]. However, little is known regarding the detailed function and regulation of ATL9 in responses against fungal pathogens. Our previous data showed that the expression of three genes, *PCC1*, *PDF1.2*, and *FBS1* were regulated by the expression of *ATL9* in response to pathogen infection [11]. *F-Box stress-induced 1 (FBS1)* is an F-box protein that is induced in response to wounding stress, osmotic stress, methyl jasmonate (MeJA), salicylic acid (SA), and abscisic acid (ABA) treatments [13]. *Pathogen and circadian controlled 1 (PCC1)*, is a pathogen-responsive gene that is regulated by the circadian clock [14]. *PCC1* is involved in the regulation of flowering time in *Arabidopsis* [14,15]. In addition, *PCC1* has also been demonstrated to operate in defense responses against the hemi-biotrophic oomycete pathogen *Phytophthora brassicae* and the necrotrophic fungal pathogen *Botrytis cinerea* [14]. *Plant defensin 1.2 (PDF1.2)*, has a myriad of functions, including response to jasmonic acid (JA) [16,17], ethylene [16], insects [18], and defense against fungal pathogens [17,18].

In this study, we have expanded on our previous work, focusing on ATL9's interacting proteins and the consequences of ATL9 overexpression [11]. Our data show that PDF1.2, PCC1 and FBS1 directly interact with and are ubiquitinated by ATL9. An in vivo ubiquitination assay showed that ATL9 can target these three proteins for degradation via the 26S proteasome. Furthermore, *atl9* T-DNA insertional mutants showed reduced expression of *PDF1.2*, *PCC1*, and *FBS1*, impairing the plant's resistance to powdery mildew. We also observed that cell death typically induced during the hypersensitive response is also associated with increased *ATL9* expression levels. Interestingly, our results also show that *ATL9* overexpression inhibits callose deposition in infected plants (Figure 7). Callose deposition is a strategy used by plants to reinforce the cell wall against penetration by fungal hyphae during infection [19,20]. Based on these data, we propose a model of the role that ATL9 may play during early infection in *Arabidopsis* and a potential mechanism demonstrating how ubiquitination, cell death and callose work together to enhance the defense response against *G. cichoracearum*.

2. Results

2.1. Mutants of *pdf1.2*, *pcc1* and *fbs1* Are More Susceptible to *G. cichoracearum* Infection

To confirm if *PDF1.2*, *PCC1* and *FBS1* are involved in defense against fungal infection, T-DNA insertional mutants of *pdf1.2*, *pcc1* and *fbs1* were infected with powdery mildew and

their phenotype was evaluated. Six days post inoculation (dpi), leaves of *atl9* (At2g35000), *pdf1.2* (AT5G44420), *pcc1* (AT3G22231), and *fsb1* (AT1G61340) all had more extensive fungal growth and the fungi had generated more spores when compared to Columbia wild type (*Col-0*), demonstrating that these mutants are more susceptible to powdery mildew infection (Figure 1). *NahG*, a transgenic plant deficient in salicylic acid (SA) production, was used as a positive control and displayed the expected hypersusceptible phenotype when infected with powdery mildew. Taken together these results indicate that *FBS1*, *PCC1* and *PDF1.2* may play a critical role in defense responses against powdery mildew.

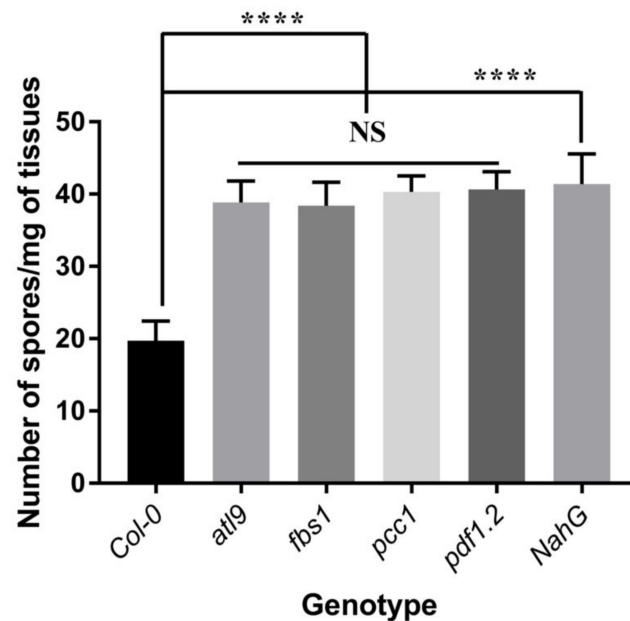


Figure 1. Quantification of *G. cichoracearum* infection on Columbia (*Col-0*) wild type and *atl9*, *fsb1*, *pcc1* and *pdf1.2* T-DNA insertional mutants. The number of spores per milligram of leaf tissue (spores/mg) was counted 6 dpi. Mutants in the four genes are significantly more susceptible to *G. cichoracearum* than *Col-0* wild-type plants. The SA-deficient *NahG* transgenic plant was used as a positive control and displayed a hypersusceptible phenotype. One-way ANOVA was used to analyze the data. The error bar indicates means \pm the SD of three independent biological replicates. **** indicates $p < 0.0001$, and NS indicates not significant. The black solid zig-zag line indicates that the significant differences are present between datasets.

2.2. *ATL9* Directly Interacts with *PDF1.2*, *FBS1*, and *PCC1*

Since mutations in *PDF1.2*, *PCC1*, and *FBS1* result in a more susceptible phenotype when challenged with powdery mildew (Figure 1), we hypothesized that the above genes may encode interacting partners of *ATL9*. To confirm this, we conducted two experiments to investigate protein-protein interactions [21,22]. In the first set of experiments, we used the yeast two-hybrid (Y2H) assay to screen for possible interactions. A combination of bait plasmid pGBKT7-*ATL9* and prey plasmids containing pGADT7-*PDF1.2*, pGADT7-*PCC1*, and pGADT7-*FBS1* were transformed into yeast strains and then mated for 12 h. SD/-Ade/-His/-Leu/-Trp/X- α -gal plates were used to indicate a positive protein-protein interaction. As shown in Figure 2, mating cultures grew on selection media and had positive β -gal activity when the *ATL9* bait (pGBKT7-*ATL9*) was combined with *PDF1.2*, *PCC1*, and *FBS1* in the prey vector. As a control, the bait plasmid pGBKT7-*ATL9* was mated with empty prey vector pGADT7 and no β -gal activity was observed (Figure 2). These data indicate that *PDF1.2*, *PCC1* and *FBS1* were strong candidates for potential interacting partners of *ATL9*.

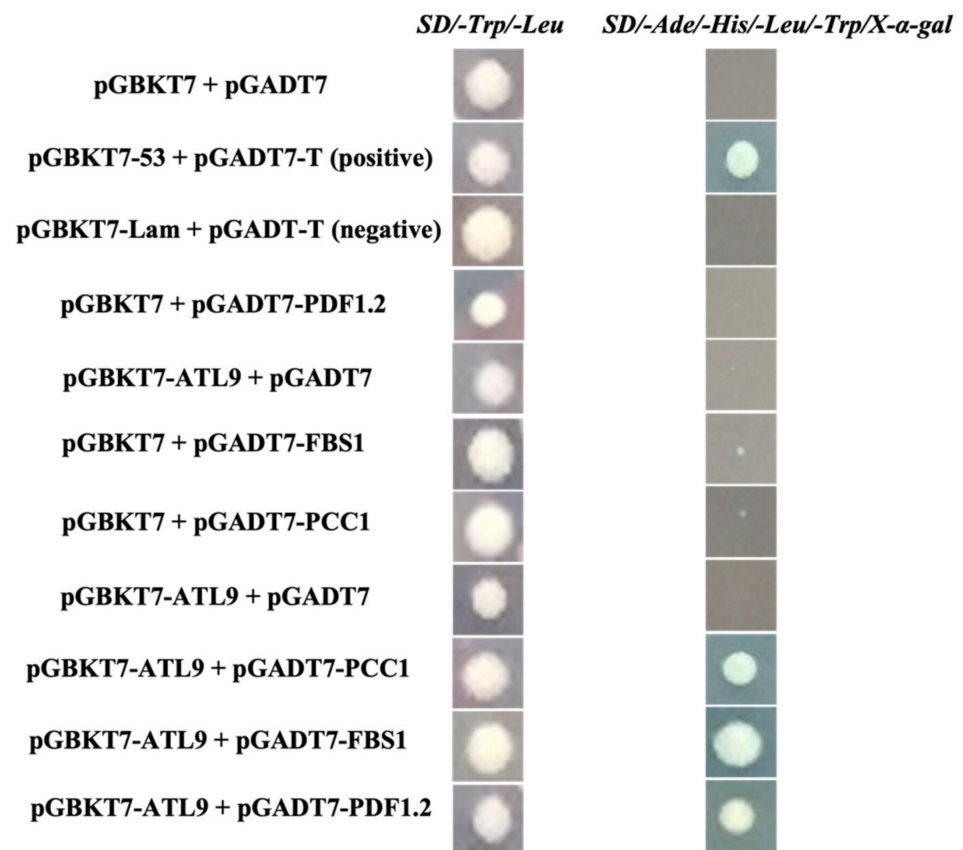


Figure 2. Yeast two-hybrid assay. The Matchmaker GAL4-Yeast two-hybrid experiments were performed as described by the manufacturer (Clontech, Mountain View, CA, USA). Positive results are indicated by blue yeast colonies and were observed in the pGBKT7-ATL9/pGADT7-FBS1, pGBKT7-ATL9/pGADT7-PCC1, and pGBKT7-ATL9/pGADT7-PDF1.2 combinations. pGBKT7-53/pGADT7-T and pGBKT7-Lam/pGADT7-T were used as positive and negative controls respectively. Experiments were repeated three times with independent samples to confirm the results.

To further investigate and confirm the interaction between ATL9 and its targets, the *in vivo* interaction observed in the Y2H assay was verified using a bimolecular fluorescence complementation assay (BiFC) [21,22]. ATL9 was fused with the C-terminal portion (amino acids 156–239) of yellow fluorescent protein (YFP; pDEST-VYCE-ATL9) and PDF1.2, PCC1, and FBS1 were fused with the N-terminal portion (amino acids 1–173) of YFP (pDEST-VYNE-PDF1.2, pDEST-VYNE-PCC1, and pDEST-VYNE-FBS1) and then co-infiltrated into *Nicotiana benthamiana* leaves. YFP fluorescence was imaged after 36 h using confocal laser-scanning microscopy (Figure 3). Results showed that YFP fluorescence was detected in cells co-infiltrated with: pDEST-VYCE-ATL9/pDEST-VYNE-PDF1.2, pDEST-VYCE-ATL9/pDEST-VYNE-PCC1, and pDEST-VYCE-ATL9/pDEST-VYNE-FBS1 reconfirming the results observed in the Y2H assays (Figure 2). No YFP fluorescence was detected in tobacco leaves co-infiltrated with only one of the constructs or with any combinations of the empty vectors (Figure S1). Together these results demonstrate that ATL9 can directly interact with PDF1.2, PCC1 and FBS1 in planta.

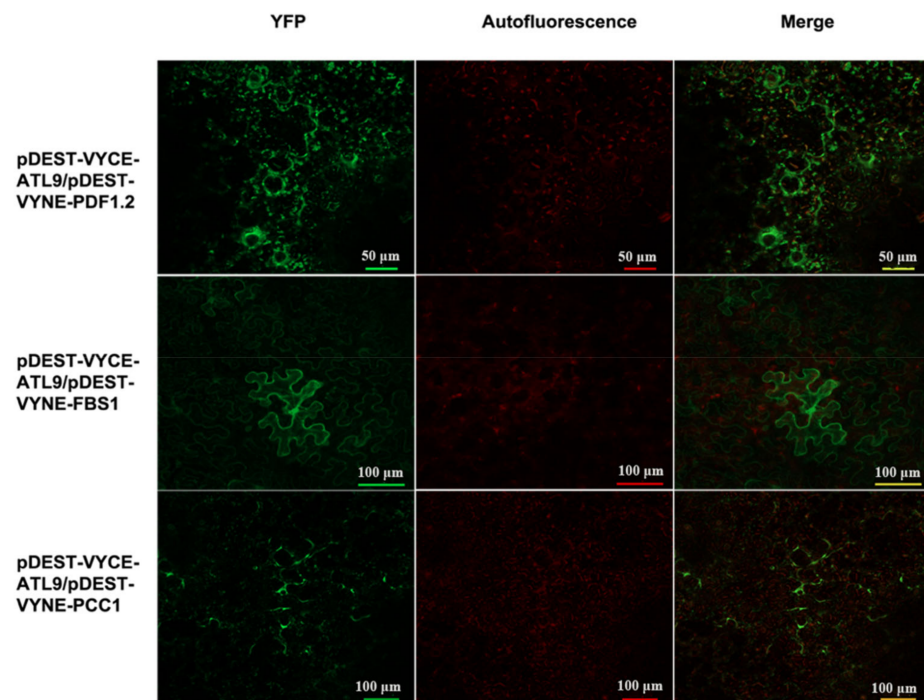


Figure 3. Bimolecular fluorescence complementation assay. pDEST-VYCE-ATL9 was transiently co-expressed with pDEST-VYNE-FBS1, pDEST-VYNE-PCC1, and pDEST-VYNE-PDF1.2 in *N. benthamiana* leaves. YFP fluorescence was observed using confocal microscopy. Yellow fluorescent emission indicated a positive interaction. FITC channel (Excitation: 460–500 nm; Emission: 510–560 nm) was used to detect YFP signal and TRITC (Excitation: 530–560 nm; Emission: 590–650 nm) filters were used to indicate autofluorescence.

2.3. *ATL9* Is Required for Degradation of *PDF1.2*, *FBS1*, and *PCC1* In Vivo

The interactions between *ATL9* and *PDF1.2*, *FBS1*, and *PCC1* shown above suggest that *ATL9* is responsible for ubiquitination of these proteins and that they are degraded via the 26S proteasome. To verify this hypothesis, we fused *PDF1.2*, *FBS1*, and *PCC1* to the green fluorescent protein (*PDF1.2*:GFP, *FBS1*:GFP, and *PCC1*:GFP) and co-infiltrated them with a vector overexpressing *ATL9* (*35S:ATL9*) in tobacco leaves. Thirty-six hours post infiltration, the transformed tobacco leaves were treated with either the protein-synthesis inhibitor cycloheximide (CHX) or a combination of CHX and MG132, a proteasome inhibitor. Fluorescent emission in the treated leaves was then monitored by confocal laser-scanning microscopy. The results are shown in Figure 4 and the white arrows indicate the areas where the protein is significantly degraded. The GFP signal fades gradually if *PDF1.2*:GFP has been co-transformed with *35S:ATL9* (Figure 4A, column I). However, if samples have been treated with CHX/MG132, the progression of the degradation is much slower, suggesting that *PDF1.2* is degraded via the 26S proteasome (Figure 4A, column II). Fluorescent emission of *PDF1.2*:GFP only or *PDF1.2*:GFP combined with an empty vector shows little to no change in degradation of the signal (Figure 4A, column III and IV). *PCC1*:GFP and *FBS1*:GFP show similar results to *PDF1.2*:GFP when co-transformed with *35S:ATL9* (Figure 4B,C). We also evaluated the influence of the individual vectors used in this experiment (Figure S2) and none of them caused any change in degradation.

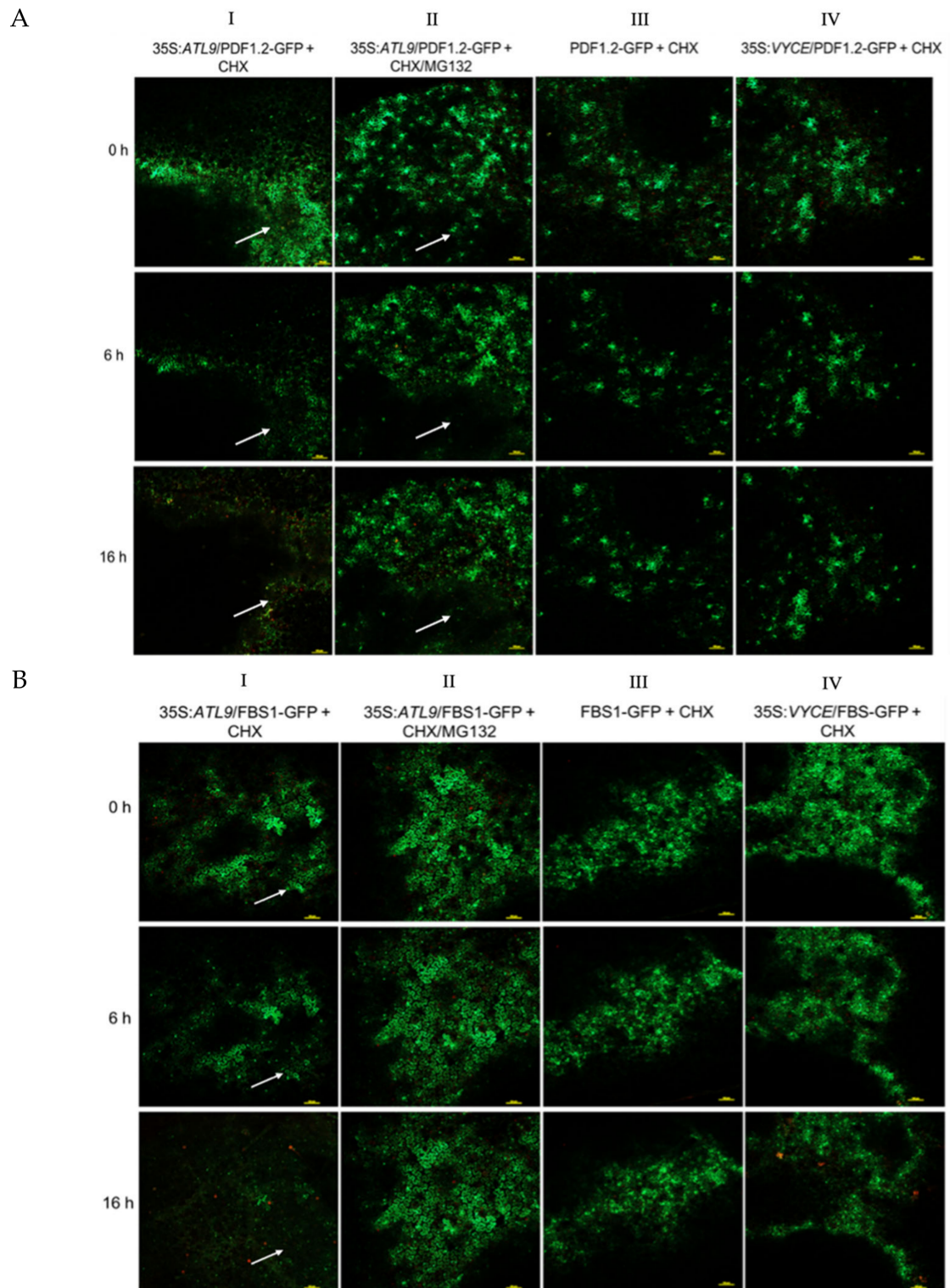


Figure 4. Cont.

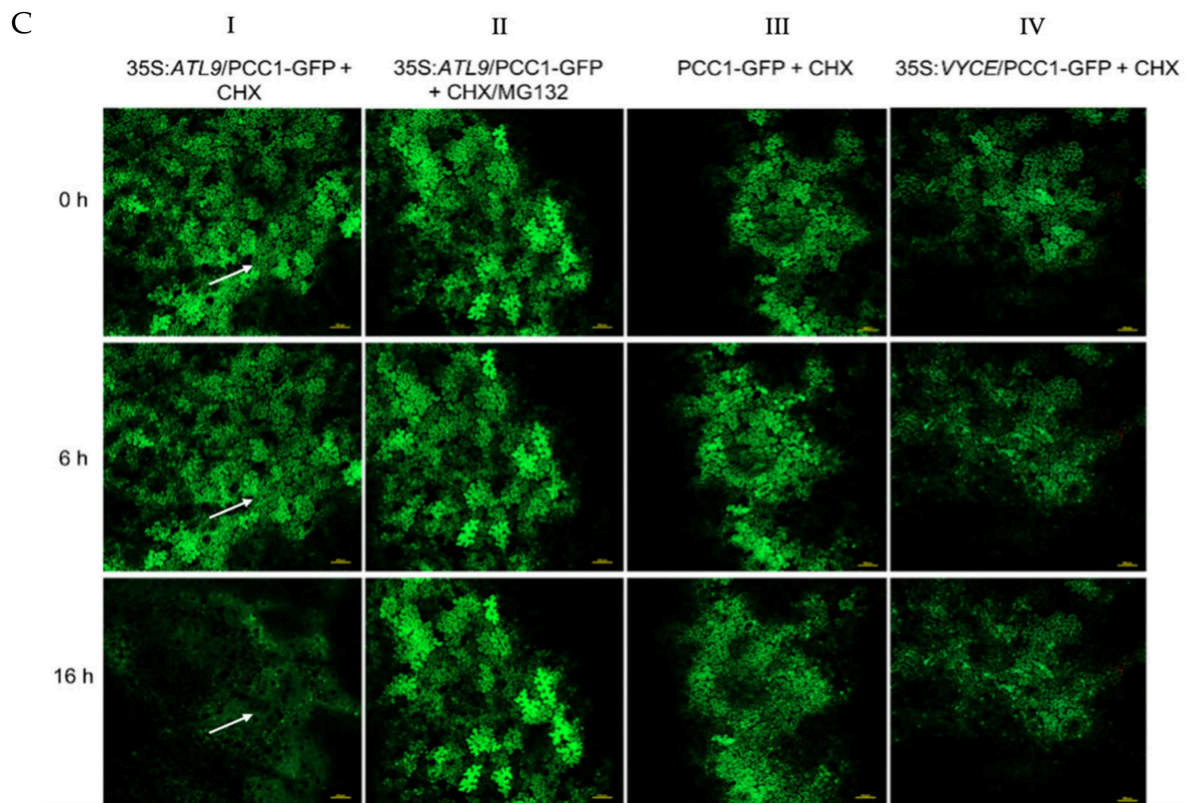


Figure 4. In vivo degradation assay. (A) 35S:ATL9 was transiently co-expressed with PDF1.2-GFP in *N. benthamiana* leaves. After 36 h incubation, leaves were treated with either 100 μ M CHX or 100 μ M CHX plus 100 μ M MG132 before observation and then fluorescence emission was monitored with the confocal microscope. Fluorescent emission of PDF1.2-GFP decreased quickly when it was co-infiltrated with 35S:ATL9 (column I). Inhibition of the 26S proteasome with MG132 significantly reduces the amount of GFP degradation, indicating that PDF1.2 is degraded via the proteasome (column II). Fluorescent emission of PDF1.2-GFP alone was persistent over the course of the experiment (column III). PDF1.2:GFP combined with an empty vector shows little to no change in degradation of the signal (column IV). The vector alone that was used for cloning ATL9 did not cause any visible degradation of PDF1.2-GFP (Figure S2). (B) 35S:ATL9 was transiently co-expressed with FBS1-GFP in *N. benthamiana*. (C) 35S:ATL9 was transiently co-expressed with PCC1-GFP in *N. benthamiana*. The FITC channel was used to detect GFP signal and the yellow scale bar indicates 100 μ m. The white arrows indicate the areas where the protein is significantly degraded.

To further verify that degradation of the three genes is caused by ATL9 alone, total protein was extracted from co-infiltrated tobacco leaves at 0 and 6 h followed by immunoblotting using an anti-GFP antiserum. The results show that the quantity of PDF1.2-GFP, PCC1-GFP, and FBS1-GFP reduces when co-infiltrated with 35S:ATL9 (Figure 5A). While PDF1.2-GFP, PCC1-GFP, and FBS1-GFP remain unchanged without co-infiltration with ATL9 (Figure 5B). Together these findings strongly suggest that in vivo degradation of FBS1, PCC1 and PDF1.2 is mediated by ATL9 and the proteasome.

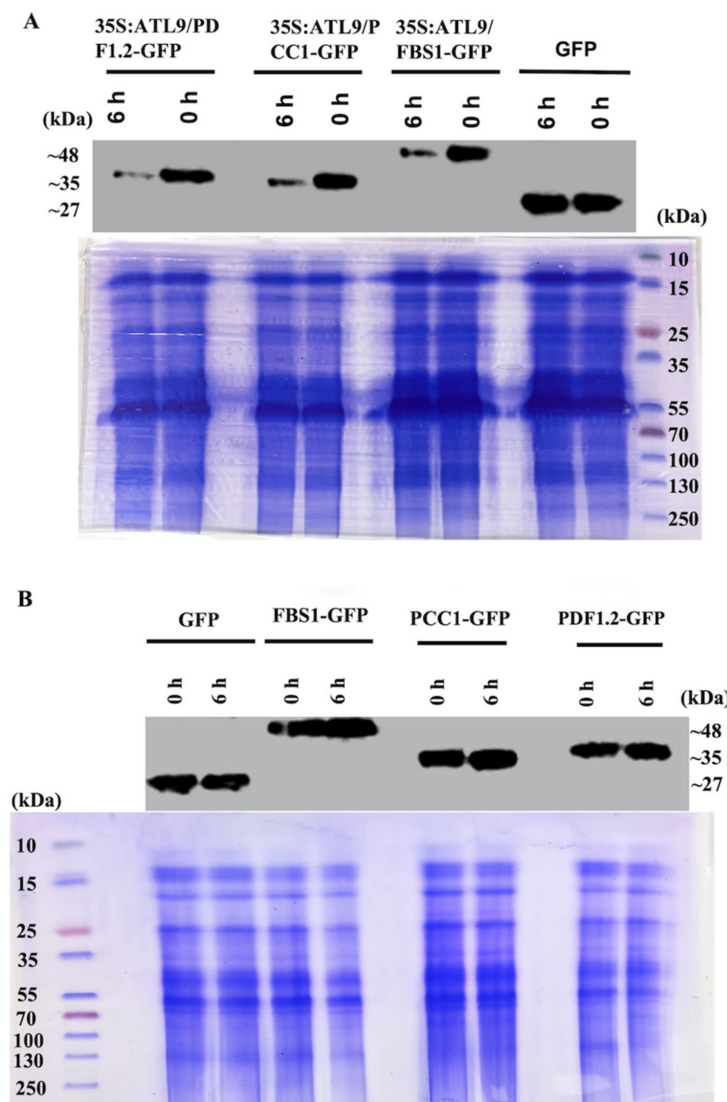


Figure 5. Immunoblotting of in vivo degradation assay. **(A)** PDF1.2-GFP, PCC1-GFP, and FBS1-GFP are co-infiltrated with 35S:ATL9. **(B)** GFP, PDF1.2-GFP, PCC1-GFP, and FBS1-GFP are infiltrated alone. Proteins were extracted from co-infiltrated tobacco leaves at 0 and 6 h after CHX treatment. Proteins were separated by SDS-PAGE and immunoblotted with anti-GFP. Samples transformed by GFP-fused vector alone were used as control. The quantity of PDF1.2-GFP, FBS1-GFP and PCC1-GFP decreased when these proteins were co-infiltrated with 35S:ATL9.

2.4. Expression Pattern of Target Genes during Plant Defense Response

Since *atl9*, *pdf1.2*, *pbs1* and *pcc1* mutants are more susceptible to *G. cichoracearum* than wild-type plants and direct interaction has been detected between ATL9 and these proteins (Figures 1–3), we were interested in investigating the expression patterns of these genes during fungal infection. *Arabidopsis* plants were inoculated with *G. cichoracearum* and leaf samples were collected at different time points after infection for RNA extraction. Quantitative analysis of the gene expression patterns reveals that, compared to *Col-0* wild-type plants (Figure 6A), the relative expression level of *PDF1.2*, *FBS1*, and *PCC1* are largely repressed in the *atl9* mutant during infection (Figure 6B). In wild-type plants, *PDF1.2* shows consistent increased expression levels across all time points sampled during infection and is highly expressed at the twenty-four hour time point, as shown in Figure 5A. *FBS1* expression is highly induced at early time points (1 h and 30 min) and at the 24 h time point while *PCC1* expression was also highly induced at early time points (1.5 h and

2 h) and at the 16 h time point. However, expression levels of all three genes showed altered patterns in the *atl9* mutant compared with Col-0 wild-type (WT) during fungal infection. As shown in Figure 6B, *FBS1* was induced at early time points (1.5 h and 2 h), but expression of *FBS1* was repressed 4 h post-fungal infection. Interestingly *PCC1* expression was decreased across most of the time points during infection. In addition, *PDF1.2* expression was significantly decreased in the *atl9* mutant compared to Col-0 during fungal infection. However, *PDF1.2* expression was induced at later time points (4 h, 16 h, and 24 h) in the *atl9* mutant after fungal infection. Together these results indicate that *ATL9* is influencing the up regulation of *PDF1.2* and *PCC1* during defense responses against powdery mildew and it is important for the increased expression levels of *FBS1* observed at early time points after the initial infection.

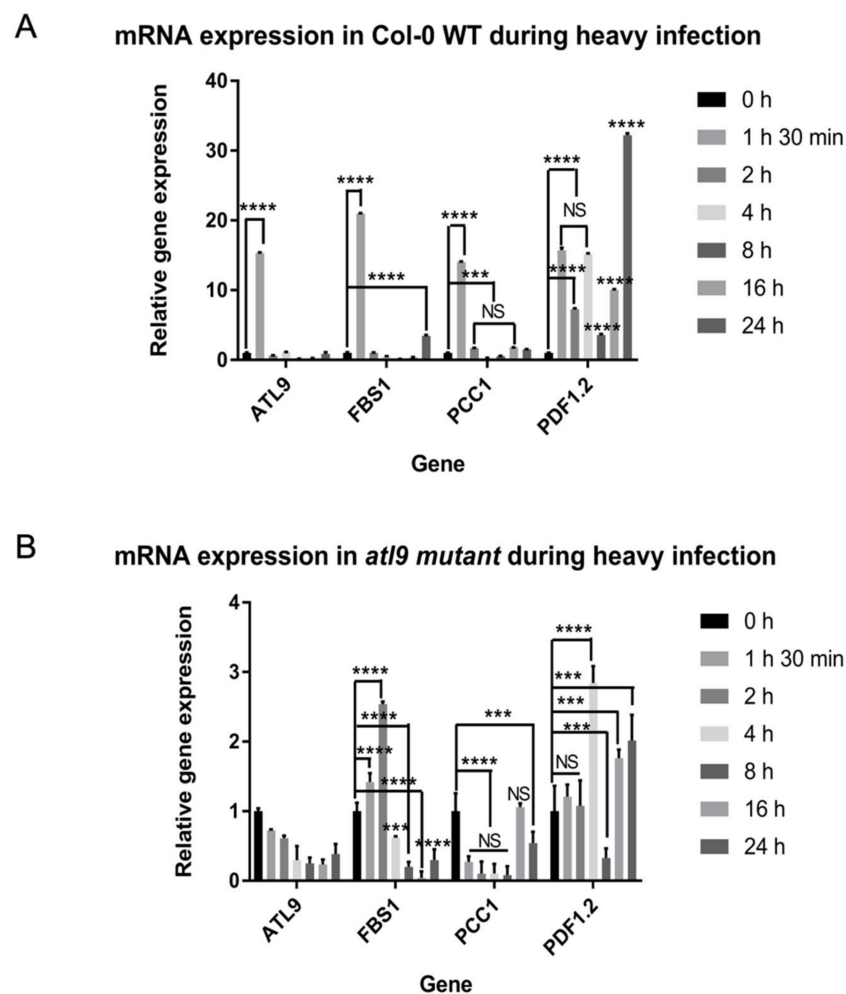


Figure 6. Expression of *ATL9*, *FBS1*, *PCC1* and *PDF1.2* in Columbia wild type and *atl9* plants after infection with *Golovinomyces cichoracearum*. (A) mRNA expression of *PDF1.2*, *FBS1*, *ATL9*, and *PCC1* in Col-0 wild type plants after heavy infection with powdery mildew. (B) mRNA expression of *PDF1.2*, *FBS1*, *ATL9*, and *PCC1* in the *atl9* mutant after heavy infection with powdery mildew. Beta-actin was used as an endogenous control. Please note change in y-axis scales between (A) and (B). Asterisks indicate statistically significant differences between the samples treated and untreated, according to One-way ANOVA analysis and multiple comparison post-Tukey's test. The experiments were repeated three times with independent biological samples. **** indicates $p < 0.0001$, *** indicates $p < 0.001$, and NS indicates not significant. The black solid zig-zag line indicates that the significant differences are present between datasets.

2.5. Deposition of Callose during Fungal Infection

Callose is a polysaccharide that plays an important role in a variety of processes during plant development and in defense responses [23]. Previous research has shown that callose is deposited in the leaf early in the infection process and can efficiently prevent fungal penetration [24]. Furthermore, callose and callose synthase have been identified as negative regulators of the SA defense pathway [25]. SA can mediate a diverse set of defense genes, is involved in cell death responses, and has significant cross talk with both the JA and ethylene defense signaling pathways [26]. Given that FBS1, PCC1, and PDF1.2 are known to be involved in SA, JA, and ethylene signaling and are targeted for degradation by ATL9, we wanted to determine if callose deposition was altered in mutants of any of these four genes [27–29].

Arabidopsis plants were infected with powdery mildew and leaf tissue was collected at four different time points after infection (3 h, 6 h, 12 h and 5 days). Callose deposition was determined by aniline blue staining and leaf samples were observed using confocal microscopy. The images of callose staining of leaves after infection for 3, 6 and 12 h or 5 days is shown in Figure 7A–D, and a quantitative assessment of the number of callose deposits per mm² leaf tissue is shown in Figure 7E. The results showed that there were different patterns of callose deposition depending on the mutant and timepoint that were being observed. After 3 h of infection, more callose deposition was observed in mutants of *atl9*, *fbs1*, *pcc1*, and *pdf1.2* compared to *Col-0* controls, while very little callose deposition was detected in 35S:*ATL9*, as shown in Figure 7A. Six hours post infection, callose deposition largely increases in all mutants tested, but more callose deposition can be observed in *Col-0*. Meanwhile, at the 6 h timepoint there is no callose observed in the 35S:*ATL9* overexpression line (Figure 7B). Callose deposition continues to increase in *Col-0* and *atl9* 12 hours-post-infection and a small amount of callose deposition was observed in the 35S:*ATL9* line at the 12 h time point (Figure 7C). In contrast, callose deposition declines at the 12-hour time point in the *fbs1*, *pcc1* and *pdf1.2* mutants relative to *Col-0* (Figure 7C). We also examined samples 5 days post infection, in order to evaluate callose deposition at a late time point in the infection progression. As shown in Figure 7D, the *ATL9* overexpression mutant has more callose deposition compared to *Col-0*, while callose deposition has been largely repressed in the *atl9*, *fbs1*, *pdf1.2* and *pcc1* mutant lines in response to fungal infection.

In summary, mutants of *pdf1.2*, *fbs1* and *pcc1* have more callose deposition at early stages of infection (6 h) while the overexpression line of *ATL9* displays more callose deposition during the late stages of infection (5 days). Callose deposition in mutants of *atl9*, *fbs1*, *pcc1* and *pdf1.2* largely decreases at later time points during infection and is much less than that seen in wildtype control leaves. In addition, callose deposition in the 35S:*ATL9* over-expression line was highly induced. These results indicate that mutants of *atl9*, *fbs1*, *pcc1* and *pdf1.2* can synthesize and accumulate more callose at earlier time points after infection with powdery mildew than *Col-0* and 35S:*ATL9* over-expression plants. Callose deposition in 35S:*ATL9* plants is apparently delayed, suggesting that less callose deposition at the points of hyphal penetration may facilitate the delivery of other plant defense compounds during early infection stages.

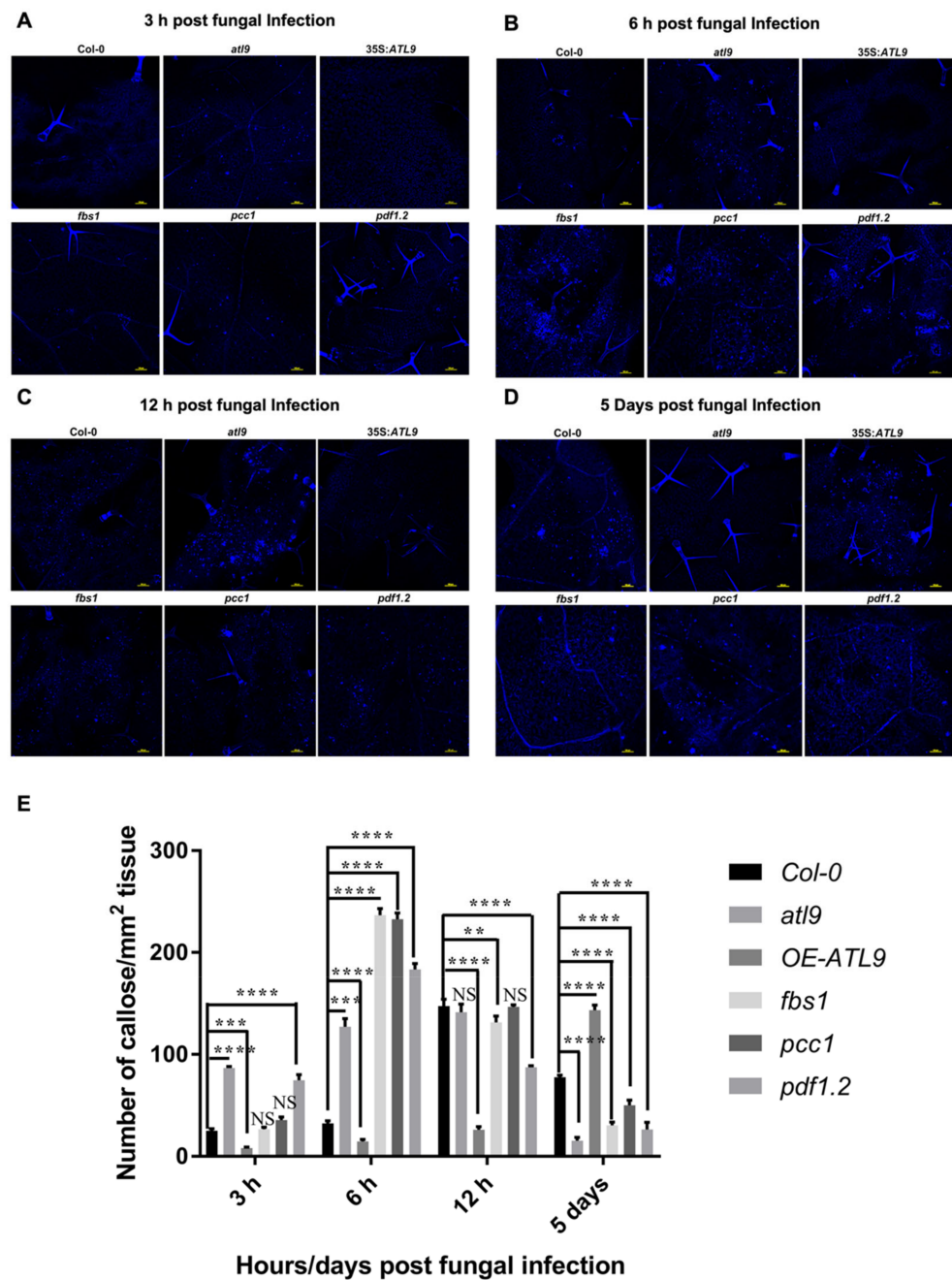


Figure 7. Callose staining of leaves after infection for 3, 6 and 12 h or 5 days post infection with powdery mildew. Plants infected with powdery mildew after (A) 3 h (B) 6 h (C) 12 h and (D) 5 days had leaves harvested and then stained for callose deposition with aniline blue. After staining, samples were observed using confocal microscopy. (E) Quantitative assessment of the number of callose deposits per mm² leaf tissue. Asterisks indicate statistically significant differences between the samples treated and untreated, according to One-way ANOVA analysis and multiple comparison post-Tukey's test. **** indicates $p < 0.0001$, *** indicates $p < 0.001$, ** $p < 0.01$ and NS indicates not significant. The black solid zig-zag line indicates that the significant differences are present between datasets. Yellow scale bars equal to 100 μm .

2.6. Cell Death during Fungal Infection

Previous studies showed that *FBS1*, *PCC1*, and *PDF1.2* are involved in the three major defense pathways mediated by SA, JA and ethylene [14,27]. The expression levels of *FBS1*, *PCC1*, and *PDF1.2* are reduced in the *atI9* mutant during fungal infection, suggesting that

ATL9 might be involved in the regulation of these hormonal pathways via interaction with *FBS1*, *PCC1*, and *PDF1.2*. Additionally, previous research in our lab has shown that induction of *ATL9* is dependent on the production of reactive oxygen species (ROS) [11]. Recent studies have indicated that treating plants with SA and JA will induce cell death [30] and that increasing ROS will elevate cell death [31]. Host cell death is known to be an important response used to limit nutrient supply to biotrophic pathogens such as powdery mildew during infection [3,4,6]. Therefore, we hypothesize that cell death may be involved in and associated with expression of *ATL9* during the early stages of infection. To verify this prediction, leaves were infected with powdery mildew for 5 days and then stained with trypan blue to observe cell death (Figure 8). Results showed that *35S:ATL9* plants displayed a higher level of trypan blue staining which equates to more cell death in the leaves of the *ATL9* overexpression plants. Meanwhile, signs of cell death in *atl9* loss of function mutants were lower than that observed in *fbs1*, *pcc1* and *pdf1.2* and more similar to the pattern observed in Col-0 wild-type. In addition, the *fbs1*, *pcc1* and *pdf1.2* mutants showed increased cell death compared to Col-0 but less than what was observed in *35S:ATL9* plants (Figure 8). Collectively, these results indicate that increased expression levels of *ATL9* do stimulate cell death and decreased or no expression of *FBS1*, *PCC1* and *PDF1.2* will also result in increased cell death in *Arabidopsis*. In summary, we predict that during early infection induction of *ATL9* is responsible for targeting *FBS1*, *PCC1*, and *PDF1.2* for degradation to the 26S proteasome to promote cell death in the leaf epidermal cells that are points of hyphal penetration to limit fungal infection.

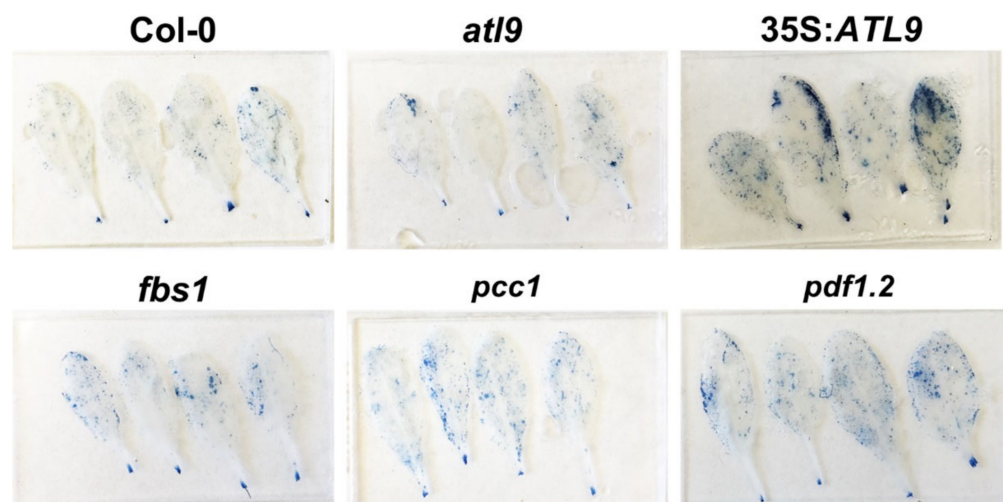


Figure 8. Cell death in leaves indicated by trypan blue staining. Plants were infected with powdery mildew for 5 days and leaf tissues were collected and stained with trypan blue. Results show that cell death in leaf epidermal cells is largely increased in *35S:ATL9* plants and slightly increased in *fbs1*, *pcc1*, and *pdf1.2* mutants.

3. Discussion

In the current work we have expanded on our previous studies, focusing on proteins that interact with the E3 ligase *ATL9*. We present evidence, via bimolecular fluorescence complementation assay and yeast-two hybrid assay, that the proteins *PDF1.2*, *PCC1* and *FBS1* directly interact with *ATL9* (Figures 3–6). Our previous work showed that *ATL9* is localized to the endoplasmic reticulum [11]. *PDF1.2* was found to localize to the ER bodies [32], where it can be secreted into the apoplasmic space after a fungal infection [33]. *PCC1* is localized to the plasma membrane [29] and *FBS1* is predicted to localize to the mitochondria based on Y2H co-expression studies [34]. A future avenue of study would be to investigate the protein ubiquitination patterns of *ATL9* and to determine the precise amino acid location of ubiquitination in *FBS1*, *PCC1* and *PDF1.2*. The detailed roles of *PCC1*,

PDF1.2, and *FBS1* in powdery mildew infection still largely remain unknown. Experiments involving multiple mutants of *pdf1.2*, *pcc1* and *pbs1* and overexpression lines of each gene are needed to provide more comprehensive information on the precise role of *ATL9*, *PCC1*, *PDF1.2*, and *FBS1* in immune responses against fungal pathogens.

The SA, JA and ethylene defense pathways are well-defined but the points of crosstalk between them during infection are still unclear. Crosstalk between different hormonal defense pathways is hypothesized to reduce allocation costs by repression of unnecessary defenses [35]. For example, signaling crosstalk between SA and JA commonly shows reciprocal antagonism [36]. Research has shown that SA, JA, and ethylene are all positive regulators of cell death in plants and that targeted cell death (the hypersensitive response) is used as a mechanism to minimize infection at limited sites in the leaf [26,37–39]. *FBS1*, *PCC1*, and *PDF1.2* are known to be involved in all three major defense pathways [14,27,40] and our data suggest that *ATL9* could be involved in adjusting SA, JA and ethylene responses through its interactions with *FBS1*, *PCC1*, and *PDF1.2*. However, further evidence is needed to definitively show the connection between these proteins and SA-, JA-, and ethylene-mediated signaling during fungal infection.

Our data show that overexpression of *ATL9* confers resistance to powdery mildew [11,12]. Expression of *ATL9*, *FBS1*, *PCC1*, and *PDF1.2* has also been shown to be important for defense responses during fungal infection, and our current data show that *ATL9* can directly bind to *FBS1*, *PCC1* and *PDF1.2* (Figures 2 and 3) and target them for degradation to the proteasome (Figures 4 and 5). In the current study, *ATL9* expression was induced only at early time points after fungal infection (Figure 6A). In contrast, *PDF1.2* expression was induced across all time points sampled during infection, *FBS1* expression was highly induced at the early time points (1 h and 30 min) and at the latest time point (24 h), while *PCC1* expression was also highly induced at the early time points (1.5 h and 2 h) and at the 16 h time point (Figure 6A). In the *atl9* loss-of-function mutant, expression levels of all genes showed altered expression patterns compared to Col-0 wild type during fungal infection, except for *PCC1* (Figure 6B). Considering all these data, we hypothesize that expression of *ATL9*, *PDF1.2*, *PCC1*, and *FBS1* during fungal infection may have complex regulation mechanisms and that *PDF1.2*, *PCC1*, and *FBS1* expression might also be regulated by other signaling pathways (or molecules) during infection. Moreover, our previous study showed that *ATL9* is also a short-lived protein within plant cells and it is degraded via the ubiquitin 26S proteasome pathway [12]. Together, this suggests that ubiquitination of *PDF1.2*, *PCC1* and *FBS1* proteins by *ATL9* is likely not a continuous process during the plant defense response [41,42]. Further results show that fungal infection triggers increased expression of *ATL9*, *FBS1*, *PCC1* and *PDF1.2* and that *atl9* loss-of-function mutants show transcriptional repression of these three genes during infection. These results indicate that *ATL9* plays a role in the upregulation of these genes at least at early timepoints during fungal infection. It appears that degradation of *FBS1*, *PCC1*, and *PDF1.2* influences other aspects of the plant defense response. Since all genes tested were highly induced at early time points post infection, further studies that focus on exploring other known early-activated defense genes and pathways that may be affected by or interact with *ATL9*, *PDF1.2*, *PCC1* and *FBS1* will allow us to construct a more detailed picture of the intersecting early responses being coordinated against fungal infection in plants.

Since *ATL9* is largely induced at early time points after infection, we also examined callose deposition in *atl9*, *pdf1.2*, *pbs1* and *pcc1* during early stages of infection. Our results show that mutants of *atl9*, *pdf1.2*, *pbs1* and *pcc1* have more callose deposition early in infection, while callose deposition was largely repressed in 35S:*ATL9* overexpression lines in response to fungal infection. This suggests that *ATL9*, *FBS1*, *PCC1*, and *PDF1.2* might negatively regulate callose deposition during early infection stages. However, callose deposition was significantly increased in the overexpression line of *ATL9* at late timepoints after infection (16 h and 24 h) and was decreased in the mutant lines. Callose deposition during infection would block successful fungal penetration and colonization of the leaf tissue and our results showed that *atl9*, *pbs1*, *pcc1* and *pdf1.2* mutants were more susceptible

to powdery mildew (Figure 1). Thus, it seems likely that *ATL9*, *FBS1*, *PCC1*, and *PDF1.2* play a more complex role in the regulation of callose deposition in response to fungal infection. Especially considering our findings that *ATL9*, *FBS1*, *PCC1* and *PDF1.2* are all highly induced 1.5 h after infection (Figure 6A) but that their expression levels are significantly decreased at the two hour timepoint (with the exception of *PDF1.2*) and remain repressed through the 24 h timepoint. Further experiments would be necessary to investigate the precise timing of *ATL9* ubiquitination of these proteins to show that *FBS1*, *PCC1* and *PDF1.2* are influencing callose deposition.

Taking the data in the current study into consideration, we propose a putative model for *ATL9*'s function in defense responses against fungi and its possible interaction with other major defense pathways (Figure 9).

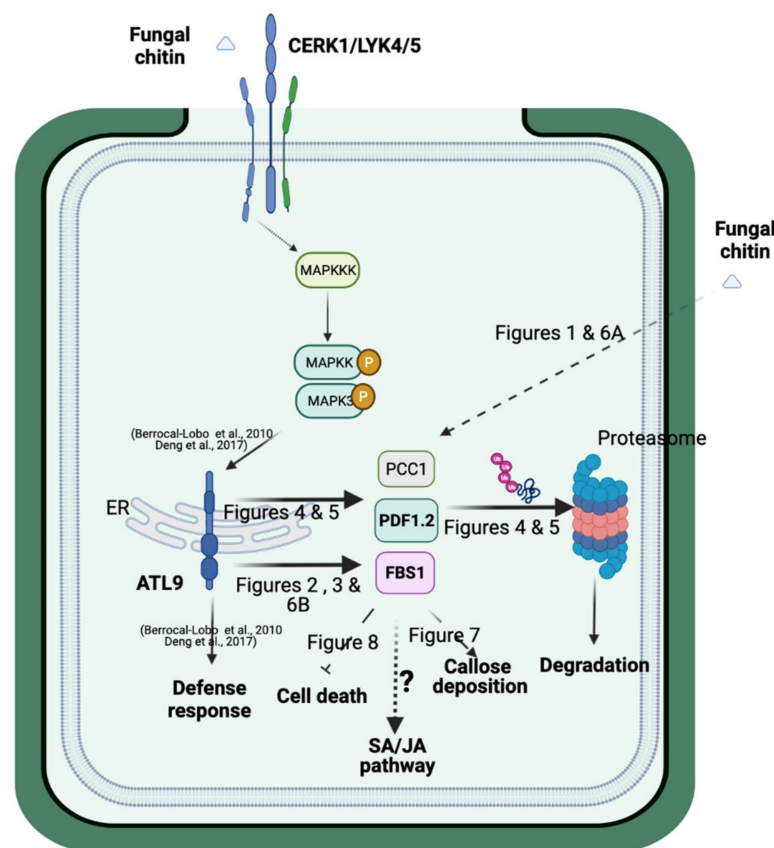


Figure 9. Schematic model of *ATL9*'s function in plant defense response. Representation of the possible role of *ATL9* during plant defense responses to fungi [11,12]. Black arrows indicate positive regulation, whereas black end-blocked lines indicate negative regulation. Dashed lines indicate possible interactions with pathways or molecules. The figure was created with BioRender.com with license agreement number FV2337XIIK (accessed on 18 October 2021).

During early infection stages, *ATL9* is highly induced after the plant is exposed to the pathogen and the classical defense pathways (SA, JA, ethylene) are activated. *FBS1*, *PCC1*, and *PDF1.2* are also upregulated (Figure 6A). Since *ATL9* can bind and degrade all three of these proteins, cell death during the early stages of infection remains active. Because *ATL9* is only significantly induced at very early time points during infection, the levels of *FBS1*, *PCC1* and *PDF1.2* will begin to accumulate over time as the infection progresses. Our callose staining results show that *atl9*, *fsb1*, *pcc1*, and *pdf1.2* all exhibit faster callose deposition compared to Col-0 during early infection (Figure 7). This indicates that *ATL9*, *FBS1*, *PCC1* and *PDF1.2* may also be involved in impeding callose deposition at sites of potential hyphal penetration. Previous studies have shown that callose and callose synthase are negative regulators of the SA pathway. Therefore, we suggest that

ATL9 might be influencing the SA, JA and ethylene pathways through the degradation of *FBS1*, *PCC1*, and *PDF1.2*. Trypan blue staining of powdery mildew infected leaf tissue showed that mutants of *fbs1*, *pcc1* and *pdf1.2* exhibit slightly more cell death than Col-0 and the *atl9* mutant (Figure 8). This indicates that *FBS1*, *PCC1* and *PDF1.2* may also be involved in the regulation of cell death during fungal infection. Combining the observed results from the callose and trypan blue staining, we predict that *ATL9*, *FBS1*, *PCC1*, and *PDF1.2* appear to be important in two distinct phases of the fungal infection process: first during the initial phase of infection and second during the propagation of the infection. During the initial phases of infection, *FBS1*, *PCC1* and *PDF1.2* are significantly induced after increased expression of *ATL9*. Cell death during the initial infection period will be activated once *FBS1*, *PCC1* and *PDF1.2* are degraded by *ATL9* via the proteasome. However, since *ATL9* is only highly expressed at very early points during infection, *FBS1*, *PCC1* and *PDF1.2* will begin to re-accumulate in plant cells as the infection progresses and then begin to inhibit callose deposition. Inhibition of callose deposition will trigger cell death via activation of the SA pathway [43,44]. It is of interest to note that *PDF1.2* is continuously induced in Col-0 plants after infection, suggesting that induction of *PDF1.2* may be involved not only in the early defense response, but also in later downstream responses involved in the persistence or propagation of the defense response. In summary, our study has shown that the E3 ubiquitin ligase *ATL9* can affect the expression of defense related genes, localized cell death, and callose deposition in response to fungal infection. These data indicate that *ATL9* may have more broad reaching effects in regulating cellular activities during fungal infection.

4. Materials and Methods

4.1. Biological Materials

All experiments were conducted with *Arabidopsis thaliana* ecotype Col-0. T-DNA insertional mutants were obtained from the Arabidopsis Biological Resource Center (ABRC, Ohio State University, Columbus, USA). To identify homozygous T-DNA mutants, PCR reactions were performed using the following primers:

pdf1.2 (Salk_063966 exon):

LP 5'-AGATAAGATGCACCGTCGATG-3'

RP 5'-ATTTGTTTCGACGATGACGAAG-3'

BP 5'-GCGTGGACCGCTTGCTGCAACT-3'

pcc1 (Sail_705_G06 promoter):

LP 5'-TTGATGATGCACCAACTTTG-3'

RP 5'-TATTGGCAGTTGTATCCAGGG-3'

BP 5'-TAGCATCTGAATTCATAACCAATCTCGATACAC-3'

fbs1 (Sail_535_D08 promoter):

LP 5'-TCTCTGTTTCACGGTGTCTCC-3'

RP 5'-TTGTGGGAAATGAACAAAAGC-3'

BP 5'-TAGCATCTGAATTCATAACCAATCTCGATACAC-3'

Mutants of *atl9* and *ATL9* overexpression line were verified from our previous research [11,12]. Plants were grown under controlled conditions in a growth chamber at 22 °C day/19 °C night with 16 h of light per 24 h and 50% relative humidity. The fungal pathogen used in this work was *Golovinomyces cichoracearum* UCSC1. *G. cichoracearum* was cultured on cucumber (*Cucumis sativus*) and maintained at 22 °C day/19 °C night with 16 h of light per 24 h and 85% relative humidity. Fungal inoculums were prepared, and inoculations performed as described [45].

4.2. Disease Assessments

Powdery mildew inoculations and disease assessments were carried out as described [45]. *Arabidopsis* seeds were planted in soil and grown in a growth chamber, as described previously. Col-0 and salicylic-acid-impaired *NahG* plants were planted as controls. After four weeks, plants were inoculated with powdery mildew and placed in a chamber under the same temperature and light conditions but with 85% relative humidity. Disease

development was assessed in a qualitative manner by tracking the appearance of powdery mildew symptoms on inoculated leaves over a period of 10 days post inoculation. Leaves at 6 days post inoculation (dpi) were harvested and infected leaf tissue was collected and weighed. Infected leaf tissue (500 mg) was placed in a 15 mL falcon tube containing 5 mL of distilled water. Fungal spores were then suspended in the distilled water by vortexing leaf tissue for approximately 1 minute. The dH₂O/spore supernatant was then decanted to a fresh tube for quantification. Spores were then quantified using a counting chamber (20 µL of supernatant/chamber), and the results were standardized as spores per mg of leaf tissue [46]. Each experiment was repeated three times and results were analyzed using a student's *t*-test.

4.3. Yeast Two-Hybrid Screening for Protein-Protein Interaction

The Matchmaker GAL4-based Yeast two-hybrid experiments were performed as described by the manufacturer (Clontech, Mountain View, CA, USA). Full-length cDNA of *ATL9* (At2g35000) was amplified from *Arabidopsis* genomic DNA using primers containing NdeI and PstI restriction enzyme sites. Primer sequences are as follows:

5'-GGAATTCATATGCAAACCAGACGTTGACTCTCTCTA-3' (Forward);

5'-AACTGCAGAAACGCAAATAAGAGGCATGACAA-3' (Reverse).

PCR products were recombined with pGBKT7 by restriction enzyme digestion to generate the binding domain construct (pGBKT7-ATL9). After confirming the sequence correctness and direction, the recombinant construct was then transformed into yeast strain Y2H Gold as bait. Full-length cDNA of *PDF1.2*, *PCC1* and *FBS1* were then cloned into pGADT7 to generate the activation domain as described above (pGADT7-PDF1.2, pGADT7-PCC1, and pGADT7-FBS1). The following gene specific primers were used for cloning:

PDF1.2 (At5g44420):

5'-CCGGAATTCACACAACACATACATCTATACATTGA-3' (Forward)

5'-CGCGGATCCACACACGATTTAGCACCAAAGATT-3' (Reverse)

PCC1 (At3g22231):

5'-CCGGAATTCCAAATCTCACATCCTCACTCCTCA-3' (Forward)

5'-CGCGGATCCAACGACTTCTGTCTCATCATGCT-3' (Reverse)

FBS1 (At1g61340):

5'-CCGGAATTCCTCAGCTTTTGTTCATTTCCAC-3' (Forward)

5'-CGCGGATCCTCCCATAGAGTTTGTGACCT-3' (Reverse)

The above recombinant constructs were then transformed into yeast strain Y187 as prey using the small-scale transformation procedure as described by the manufacturer (Clontech, Mountain View, CA, USA (accessed on 18 March,2018); <https://www.takarabio.com>) (accessed on 18 March 2018).

Y187 preys (in pGADT7) and Y2H Golds bait(pGBKT7-ATL9) cultures were mixed and mated overnight (20–24 h) with shaking at 200 rpm at 30 °C. Prey pGADT7-T and bait pGBKT7-53 was used as a positive control and prey pGADT7-T and bait pGBKT7-Lam was used as a negative control. For false positive interactions, empty pGBKT7 was mixed with preys (in pGADT7) and empty pGADT7 was mixed with baits (pGBKT7-ATL9). After a 20-h incubation, the mated yeast strains were spread on selective plates with SD/-Leu/-Trp and then SD/-His/-Leu/-Trp medium. The positive colonies were picked and then cultured at SD/-Ade/-His/-Leu/-Trp/X-α-gal plates. Plates were incubated for 3–5 days at 30 °C to screen for blue positive colonies, indicating protein-protein interactions (Clontech).

4.4. Bimolecular Fluorescence Complementation Assays

To confirm the results of the Y2H assay, bimolecular fluorescence complementation (BiFC) assays were also conducted with constructs of pDEST-VYCE and pDEST-VYNE [47]. *ATL9*, *PDF1.2*, *PCC1* and *FBS1* were amplified by PCR as described above. An adenine (A) overhang was added to the amplified PCR products using Taq polymerase and then the constructs were cloned into the PCR8/TOPO/GW entry vector (Invitrogen, Carlsbad, CA).

pDEST-VYCE-ATL9, pDEST-VYNE-PDF1.2, pDEST-VYNE-FBS1, and pDEST-VYNE-PCC1 were then generated by LR reaction (Invitrogen, Carlsbad, CA, USA). All constructs were transformed into *Agrobacterium tumefaciens* strain GV3101 using the freeze/thaw method. Cultured *A. tumefaciens* cells were harvested at OD₆₀₀ = 1.0 and then were re-suspended in fresh infiltration media (containing 10 mM MES/KOH (pH 5.6), 10 mM MgCl₂, and 150 µM acetosyringone) to yield a final OD₆₀₀ of ~0.5. Re-suspended cultures were incubated for another 2 h at 28 °C with moderate shaking (75 rpm) in darkness [21]. The BiFC partner strains were co-infiltrated into *Nicotiana benthamiana* leaves using a blunt syringe and infiltration spots were outlined using a sharpie marker. Thirty-six hours post-infiltration fluorescence was imaged in the tobacco leaves using a confocal laser-scanning microscope (Nikon Eclipse Ti2, Tokyo, Japan). For the confocal laser-scanning microscopy, two filters were used, the FITC filter (Excitation: 460–500 nm; Emission: 510–560 nm) and the TRITC filter (Excitation: 530–560 nm; Emission: 590–650 nm) (Nikon, Tokyo, Japan). Images were generated and merged using NIS-Elements software Version 4.60.00 (Nikon, Tokyo, Japan).

4.5. Analysis of Protein Degradation in Tobacco Leaves

For in vivo detection of ubiquitinated PDF1.2, PCC1, and FBS1, C-terminal GFP-fusion constructs of each gene (*PDF1.2-GFP*, *PCC1-GFP*, *FBS1-GFP*) were produced in the same way as the BiFC constructs, except that the destination vector used was pMDC43 (ABRC). *Agrobacterium tumefaciens* strain GV3101 containing 35S:*ATL9* and one of the recombinant GFP constructs was then co-infiltrated into tobacco leaves [21]. After 36 h incubation, leaves were treated with either the protein synthesis inhibitor cycloheximide (CHX) or CHX plus the proteasome inhibitor MG132, by immersing the infiltrated leaf in MS medium containing either 100 µM CHX or 100 µM CHX plus 100 µM MG132 for 1 h at room temperature [48]. Fluorescence was then monitored using a confocal laser-scanning microscope (Nikon Eclipse Ti2, Tokyo, Japan). For the confocal laser-scanning microscope, FITC filter (Excitation: 460–500 nm; Emission: 510–560 nm) (Nikon, Tokyo, Japan) was used to detect the GFP signal. Images were generated and merged using NIS-Elements software Version 4.60.00 (Nikon, Tokyo, Japan).

Protein degradation was also verified by immunoblotting. Co-transformed tobacco leaf samples were flash frozen using liquid nitrogen and ground into a powder after 0 and 6 h of CHX treatment. Total protein was then extracted using Tris extraction buffer [47]. Proteins were then separated by SDS-PAGE, blotted, transferred to PVDF transfer membrane and probed using polyclonal anti-GFP (Invitrogen, Carlsbad, CA, USA). Results were visualized using chemiluminescence (ThermoFisher, Waltham, MA, USA).

4.6. Gene Expression Pattern by qRT-PCR

21-day old seedlings were infected with the powdery mildew pathogen (*G. cichoracearum*) as previous described [46] and six leaves from six seedlings/genotype were randomly chosen and collected at 0-, 1.5-, 2-, 4-, 8-, 16- and 24-hours post-infection. Total RNA was isolated from infected leaf tissue using the RNeasy Plant Mini Kit (Qiagen, Germantown, MD, USA) and then treated with RQ1 DNase I (Promega, Madison, WI, USA) according to the manufacturer's protocol. First-strand cDNA was synthesized using the High Capacity cDNA Reverse Transcription Kit (Applied Biosystems, Foster City, CA, USA). The qRT-PCR was performed using iTaq™ Universal SYBR Green Supermix (BIO-RAD, Hercules, CA, USA) with reactions performed at a final volume of 10 µL per well and using the cycle protocol recommended by the manufacturer (95 °C for 2 min, 40 cycles of 95 °C for 15 s and 60 °C for 30 s, 55–95 °C for 10 s). Samples were then run using a StepOne Real-Time PCR System (Applied Biosystems, Foster City, CA, USA). Gene specific primers were designed using the Geneious program (Biomatters, Newark, NJ, USA). The following gene specific primers were used for qRT-PCR;

ATL9:

5'-TGGAAGAACGTGAAAACCTGTGC-3' (Forward)

5'-GGATCCCACACAACCTTCTCTT-3' (Reverse)

PDF1.2:

5'-TGTTCTCTTTGCTGCTTTTCGAC-3' (Forward)

5'-TGCTGGGAAGACATAGTTGCAT-3' (Reverse)

PCC1:

5'-CGTGCAAAAACCTTCAGAGACT-3' (Forward)

5'-AACTCATTATGGCTTCGGGGTT-3' (Reverse)

FBS1:

5'-CGCGTATAGTACACCTCGGAAA-3' (Forward)

5'-GAATAGAGCCACTGAGACTCCG-3' (Reverse)

Beta-Actin:

5'-CATGCCATCCTCCGTCTTGA-3' (Forward)

5'-AGCAGCTTCCATTCCCACAA-3' (Reverse)

Changes in transcript levels were determined using the $2^{-\Delta\Delta CT}$ method. Three independent biological replicates were performed for each experiment.

4.7. Trypan Blue Staining for Cell Death

Cell death was visualized in leaves via trypan blue staining [49,50]. Leaf samples were collected with scissors and the cut leaf tissue was then immersed in 2 mL of fresh trypan blue solution (lactic acid: phenol: glycerol: dH₂O = 1:1:1:1, trypan blue with final concentration of 10 mg/mL) in a culture plate for 30 min to 1 h at room temperature. Trypan blue solution was then replaced by 2 mL of 98–100% ethanol and the culture plate was allowed to sit on the bench for 2 min. The ethanol solution was then changed several times until the leaf tissue became colorless. 60% glycerol was then used to replace the ethanol and leaf samples were mounted on a microscope slide for observation.

4.8. Aniline Blue Staining for Callose Deposition

Callose deposition was observed using aniline blue staining based on standard protocols [47]. Briefly, infected leaves were harvested, placed into a culture plate and destained in lactophenol solution for 2 days at room temperature. The leaf tissue was then washed in 50% ethanol. Cleared leaf samples were then incubated in an aniline blue (MACRON, Center Valley, PA, USA) solution for 2 days in the dark at room temperature. The aniline blue staining solution was discarded and aniline blue stained leaves were then mounted onto a glass slide and observed using a confocal microscope with UV-light excitation. The number of callose deposits per leaf were counted using ImageJ software as described [51,52].

Supplementary Materials: The following are available online at <https://www.mdpi.com/article/10.3390/pathogens11010068/s1>, Figure S1: Negative control of bimolecular fluorescence complementation assay; Figure S2: Controls used in in vivo ubiquitination Assay.

Author Contributions: Conceptualization, T.G., F.K. and K.M.R.; Data curation, T.G.; Formal analysis, T.G., F.K., C.B., S.S., B.B., J.R.; Investigation, T.G., F.K. and K.M.R.; Methodology, T.G. and F.K.; Project administration, T.G. and K.M.R.; Resources, T.G.; K.M.R. Software, T.G. and F.K.; Supervision, T.G. and K.M.R.; Validation, T.G., F.K., C.B., S.S., B.B., J.R.; Visualization, T.G. and F.K.; Writing—original draft, T.G.; Writing—review & editing, T.G., F.K. and K.M.R. All authors have read and agreed to the published version of the manuscript.

Funding: This research received no external funding.

Institutional Review Board Statement: Not applicable.

Informed Consent Statement: Not applicable.

Data Availability Statement: Data is contained within the article or supplementary material.

Acknowledgments: We thank all the members of the Ramonell lab for helpful discussions and review of the manuscript.

Conflicts of Interest: The authors declare no conflict of interest.

References

1. Diaz, I. Plant defense genes against biotic stresses. *Int. J. Mol. Sci.* **2018**, *19*, 2446. [[CrossRef](#)] [[PubMed](#)]
2. Jones, J.D.; Dangl, J.L. The plant immune system. *Nature* **2006**, *444*, 323–329. [[CrossRef](#)] [[PubMed](#)]
3. Bigeard, J.; Colcombet, J.; Hirt, H. Signaling mechanisms in pattern-triggered immunity (PTI). *Mol. Plant.* **2015**, *8*, 521–539. [[CrossRef](#)]
4. Garner, C.M.; Kim, S.H.; Spears, B.J.; Gassmann, W. Express yourself: Transcriptional regulation of plant innate immunity. *Semin. Cell Dev. Biol.* **2016**, *56*, 150–162. [[CrossRef](#)]
5. McLellan, H.; Chen, K.; He, Q.; Wu, X.; Boevink, P.C.; Tian, Z.; Birch, P.R. The ubiquitin E3 ligase PUB17 positively regulates immunity by targeting a negative regulator, KH17, for degradation. *Plant Commun.* **2020**, *1*, 100020. [[CrossRef](#)] [[PubMed](#)]
6. Nguyen, Q.M.; Iswanto, A.B.B.; Son, G.H.; Kim, S.H. Recent advances in effector-triggered immunity in plants: New pieces in the puzzle create a different paradigm. *Int. J. Mol. Sci.* **2021**, *22*, 4709. [[CrossRef](#)]
7. Dielen, A.S.; Badaoui, S.; Candresse, T.; German-Retana, S. The ubiquitin/26S proteasome system in plant-pathogen interactions: A never-ending hide-and-see game. *Mol. Plant Pathol.* **2010**, *11*, 293–308. [[CrossRef](#)]
8. Gagne, J.M.; Smalle, J.; Gingerich, D.J.; Walker, J.M.; Yoo, S.D.; Yanagisawa, S.; Vierstra, R.D. Arabidopsis EIN3-binding F-box 1 and 2 form ubiquitin-protein ligases that repress ethylene action and promote growth by directing EIN3 degradation. *Proc. Natl. Acad. Sci. USA* **2004**, *101*, 6803–6808. [[CrossRef](#)]
9. Marino, D.; Peeters, N.; Rivas, S. Ubiquitination during plant immune signaling. *Plant Physiol.* **2012**, *160*, 15–27. [[CrossRef](#)]
10. Duplan, V.; Rivas, S. E3 ubiquitin-ligases and their target proteins during the regulation of plant innate immunity. *Front. Plant Sci.* **2014**, *5*, 42. [[CrossRef](#)]
11. Berrocal-Lobo, M.; Stone, S.; Yang, X.; Antico, J.; Callis, J.; Ramonell, K.M.; Somerville, S. ATL9, a RING zinc finger protein with E3 ubiquitin ligase activity implicated in chitin- and NADPH oxidase-mediated defense responses. *PLoS ONE* **2010**, *5*, e14426. [[CrossRef](#)] [[PubMed](#)]
12. Deng, F.; Guo, T.; Lefebvre, M.; Scaglione, S.; Antico, C.J.; Jing, T.; Yang, X.; Shan, W.; Ramonell, K.M. Expression and regulation of ATL9, an E3 ubiquitin ligase involved in plant defense. *PLoS ONE* **2017**, *12*, e0188458. [[CrossRef](#)]
13. Maldonado-Calderón, M.T.; Sepúlveda-García, E.; Rocha-Sosa, M. Characterization of novel F-box proteins in plants induced by biotic and abiotic stress. *Plant Sci.* **2012**, *185–186*, 208–217. [[CrossRef](#)]
14. Mir, R.; Hernández, M.L.; Abou-Mansour, E.; Martínez-Rivas, J.M.; Mauch, F.; Métraux, J.-P.; León, J. Pathogen and circadian controlled 1 (PCC1) regulates polar lipid content, ABA-related responses, and pathogen defence in Arabidopsis thaliana. *J. Exp. Bot.* **2013**, *64*, 3385–3395. [[CrossRef](#)] [[PubMed](#)]
15. Segarra, S.; Mir, R.; Martínez, C.; León, J. Genome-wide analyses of the transcriptomes of salicylic acid-deficient versus wild-type plants uncover Pathogen and Circadian Controlled 1 (PCC1) as a regulator of flowering time in Arabidopsis. *Plant Cell Environ.* **2010**, *33*, 11–22. [[CrossRef](#)] [[PubMed](#)]
16. Brown, R.L.; Kazan, K.; McGrath, K.; Maclean, D.J.; Manners, J.M. A role for the GCC-box in jasmonate-mediated activation of the PDF1.2 gene of Arabidopsis. *Plant Physiol.* **2003**, *132*, 1020–1032. [[CrossRef](#)] [[PubMed](#)]
17. Epple, P.; Apel, K.; Bohmann, H. ESTs reveal a multigene family for plant defensins in Arabidopsis thaliana. *FEBS Lett.* **1997**, *400*, 168–172. [[CrossRef](#)]
18. Moran, P.J.; Thompson, G.A. Molecular responses to aphid feeding in Arabidopsis in relation to plant defense pathways. *Plant Physiol.* **2001**, *125*, 1074–1085. [[CrossRef](#)]
19. Liu, F.; Zou, Z.; Fernando, W.G.D. Characterization of Callose Deposition and Analysis of the Callose Synthase Gene Family of Brassica napus in Response to Leptosphaeria maculans. *J. Mol. Sci.* **2018**, *19*, 3769. [[CrossRef](#)]
20. Ellinger, D.; Naumann, M.; Falter, C.; Zwikowics, C.; Jamrow, T.; Manisseri, C.; Somerville, S.C.; Voigt, C.A. Elevated early callose deposition results in complete penetration resistance to powdery mildew in Arabidopsis. *Plant Physiol.* **2013**, *161*, 1433–1444. [[CrossRef](#)]
21. Gehl, C.; Waadt, R.; Kudla, J.; Mendel, R.-R.; Hänsch, R. New GATEWAY vectors for high throughput analyses of protein-protein interactions by bimolecular fluorescence complementation. *Mol. Plant* **2009**, *2*, 1051–1058. [[CrossRef](#)]
22. Schweiger, R.; Schwenkert, S. Protein-protein interactions visualized by bimolecular fluorescence complementation in tobacco protoplasts and leaves. *J. Vis. Exp.* **2014**, *85*, 51327. [[CrossRef](#)]
23. Chen, X.-Y.; Kim, J.-Y. Callose synthesis in higher plants. *Plant Signal. Behav.* **2009**, *4*, 489–492. [[CrossRef](#)]
24. Voigt, C.A. Callose-mediated resistance to pathogenic intruders in plant defense-related papillae. *Front. Plant Sci.* **2014**, *5*, 168. [[CrossRef](#)]
25. Nishimura, M.T.; Stein, M.; Hou, B.-H.; Vogel, J.P.; Edwards, H.; Somerville, S.C. Loss of a callose synthase results in salicylic acid-dependent disease resistance. *Science* **2003**, *301*, 969–972. [[CrossRef](#)]
26. Bouchez, O.; Huard, C.; Lorrain, S.; Roby, D.; Balagué, C. Ethylene is one of the key elements for cell death and defense response control in the Arabidopsis lesion mimic mutant vad1. *Plant Physiol.* **2007**, *145*, 465–477. [[CrossRef](#)] [[PubMed](#)]
27. Gonzalez, L.; Keller, K.; Chan, K.X.; Gessel, M.M.; Thines, B.C. Transcriptome analysis uncovers Arabidopsis F-BOX STRESS INDUCED 1 as a regulator of jasmonic acid and abscisic acid stress gene expression. *BMC Genom.* **2017**, *18*, 533. [[CrossRef](#)] [[PubMed](#)]

28. Thomma, B.P.H.J.; Eggermont, K.; Penninckx, I.A.M.A.; Mauch-Mani, B.; Vogelsang, R.; Cammue, B.P.A.; Broekaert, W.F. Separate jasmonate-dependent and salicylate-dependent defense-response pathways in Arabidopsis are essential for resistance to distinct microbial pathogens. *Proc. Natl. Acad. Sci.* **1998**, *95*, 15107–15111. [[CrossRef](#)] [[PubMed](#)]
29. Mir, R.; León, J. Pathogen and circadian controlled 1 (PCC1) protein is anchored to the plasma membrane and interacts with subunit 5 of COP9 signalosome in Arabidopsis. *PLoS ONE* **2014**, *9*, e87216. [[CrossRef](#)]
30. Mur, L.A.; Kenton, P.; Atzorn, R.; Miersch, O.; Wasternack, C. The outcomes of concentration-specific interactions between salicylate and jasmonate signaling include synergy, antagonism, and oxidative stress leading to cell death. *Plant Physiol.* **2006**, *140*, 249–262. [[CrossRef](#)]
31. Van Breusegem, F.; Dat, J.F. Reactive oxygen species in plant cell death. *Plant Physiol.* **2006**, *141*, 384–390. [[CrossRef](#)]
32. Pečenková, T.; Pleskot, R.; Žárský, V. Subcellular Localization of Arabidopsis Pathogenesis-Related 1 (PR1) Protein. *Int. J. Mol. Sci.* **2017**, *18*, 825. [[CrossRef](#)]
33. Watanabe, S.; Shimada, T.; Hiruma, K.; Takano, Y. Pathogen infection trial increases the secretion of proteins localized in the endoplasmic reticulum body of Arabidopsis. *Plant Physiol.* **2013**, *163*, 659–664. [[CrossRef](#)]
34. Hooper, C.M.; Castleden, I.R.; Tanz, S.; Aryamanesh, N.; Millar, A.H. SUBA4: The interactive data analysis centre for Arabidopsis subcellular protein locations. *Nucleic Acids Res.* **2017**, *45*, D1064–D1074. [[CrossRef](#)]
35. Vos, I.A.; Amoritz, L.; Pieterse, C.; Van Wees, S.C.M. Impact of hormonal crosstalk on plant resistance and fitness under multi-attacker conditions. *Front. Plant Sci.* **2015**, *6*, 639. [[CrossRef](#)] [[PubMed](#)]
36. Thaler, J.S.; Humphrey, P.T.; Whiteman, N.K. Evolution of jasmonate and salicylate signal crosstalk. *Trends Plant Sci.* **2012**, *17*, 260–270. [[CrossRef](#)] [[PubMed](#)]
37. Morel, J.-B.; Dangl, J.L. The hypersensitive response and the induction of cell death in plants. *Cell Death Differ.* **1997**, *4*, 671–683. [[CrossRef](#)] [[PubMed](#)]
38. Brodersen, P.; Mailnovsky, F.G.; Hématy, K.; Newman, M.-A.; Mundy, J. The role of salicylic acid in the induction of cell death in Arabidopsis acd11. *Plant Physiol.* **2005**, *138*, 1037–1045. [[CrossRef](#)]
39. Reinbothe, C.; Springer, A.; Samol, I.; Reinbothe, S. Plant oxylipins: Role of jasmonic acid during programmed cell death, defence and leaf senescence. *FEBS J.* **2009**, *276*, 4666–4681. [[CrossRef](#)]
40. Leon-Reyes, A.; Van der Does, D.; De Lange, E.S.; Delker, C.; Wasternack, C.; Van Wees, S.C.M.; Ritsema, T.; Pieterse, C.M.J. Salicylate-mediated suppression of jasmonate-responsive gene expression in Arabidopsis is targeted downstream of the jasmonate biosynthesis pathway. *Planta* **2010**, *232*, 1423–1432. [[CrossRef](#)]
41. Göllner, K.; Schweizer, P.; Bai, Y.; Panstruga, R. Natural genetic resources of Arabidopsis thaliana reveal a high prevalence and unexpected phenotypic plasticity of RPW8-mediated powdery mildew resistance. *New Phytol.* **2008**, *177*, 725–742. [[CrossRef](#)]
42. Manners, J.M.; Penninckx, I.A.; Vermaere, K.; Kazan, K.; Brown, R.L.; Morgan, A.; MacLean, D.J.; Curtis, M.D.; Cammue, B.P.; Broekaert, W.F. The promoter of the plant defensin gene PDF1.2 from Arabidopsis is systemically activated by fungal pathogens and responds to methyl jasmonate but not to salicylic acid. *Plant Mol. Biol.* **1998**, *38*, 1071–1080. [[CrossRef](#)]
43. Wang, Y.; Li, X.; Fan, B.; Zhu, C.; Chen, Z. Regulation and Function of Defense-Related Callose Deposition in Plants. *Int. J. Mol. Sci.* **2021**, *22*, 2393. [[CrossRef](#)]
44. Wang, X.; Sager, R.; Cui, W.; Zhang, C.; Lu, H.; Lee, J.-Y. Salicylic acid regulates plasmodesmata closure during innate immune responses in Arabidopsis. *Plant Cell* **2013**, *25*, 2315–2329. [[CrossRef](#)] [[PubMed](#)]
45. Vogel, J.; Somerville, S. Isolation and characterization of powdery mildew-resistant Arabidopsis mutants. *Proc. Natl. Acad. Sci. USA* **2000**, *97*, 1897–1902. [[CrossRef](#)]
46. Weßling, R.; Panstruga, R. Rapid quantification of plant-powdery mildew interactions by qPCR and conidiospore counts. *Plant Methods* **2012**, *8*, 35. [[CrossRef](#)] [[PubMed](#)]
47. Glenz, K.; Bouchon, B.; Stehle, T.; Wallich, R.; Simon, M.M.; Warzecha, H. Production of a recombinant bacterial lipoprotein in higher plant chloroplasts. *Nat. Biotechnol.* **2006**, *24*, 76–77. [[CrossRef](#)] [[PubMed](#)]
48. Lee, H.I.; Raskin, I. Purification, cloning, and expression of a pathogen inducible UDP-glucose:Salicylic acid glucosyltransferase from tobacco. *J. Biol. Chem.* **1999**, *274*, 36637–36642. [[CrossRef](#)] [[PubMed](#)]
49. Mulaosmanovic, E.; Lindblom, T.U.T.; Bengtsson, M.; Windstam, S.T.; Mogren, L.; Marttila, S.; Stützel, H.; Alsanius, B.W. High-throughput method for detection and quantification of lesions on leaf scale based on trypan blue staining and digital image analysis. *Plant Methods* **2020**, *16*, 1–22. [[CrossRef](#)] [[PubMed](#)]
50. Fernández-Bautista, N.; Nuñez, J.A.D.; Moreno, M.M.; Berrocal-Lobo, M. Plant tissue trypan blue staining during phytopathogen infection. *Bio-protocol* **2016**, *6*, e2078. [[CrossRef](#)]
51. Zhou, J.; Spallek, T.; Faulkner, C.; Robatzek, S. CalloseMeasurer: A novel software solution to measure callose deposition and recognise spreading callose patterns. *Plant Methods* **2012**, *8*, 49. [[CrossRef](#)] [[PubMed](#)]
52. Zavaliev, R.; Epel, B.L. Imaging callose at plasmodesmata using aniline blue: Quantitative confocal microscopy. *Methods Mol. Biol.* **2014**, *1217*, 105–119. [[CrossRef](#)]